Electronic Supplementary Material (ESI) for Journal of Materials Chemistry C.

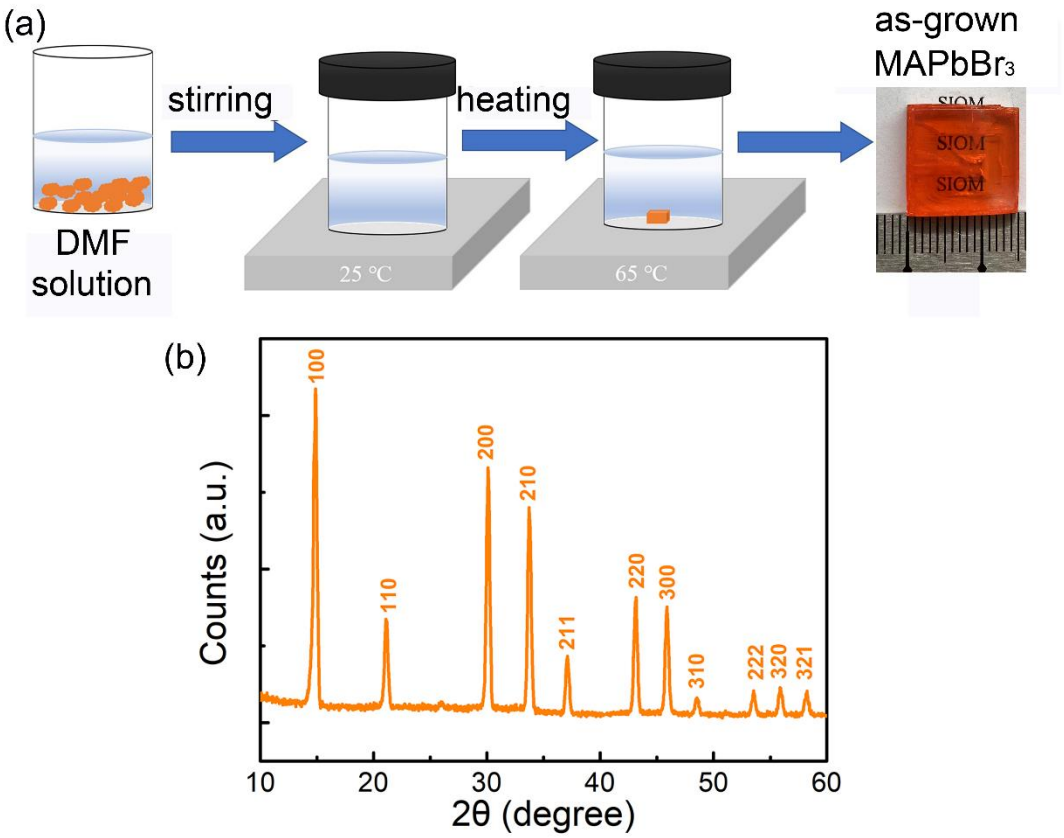

Figure S1. (a) Schematic representation of crystals growth process based on inversion temperature crystallization (ITC). (b) Powder X-ray diffraction of as-grown $MAPbBr_3$ crystals.

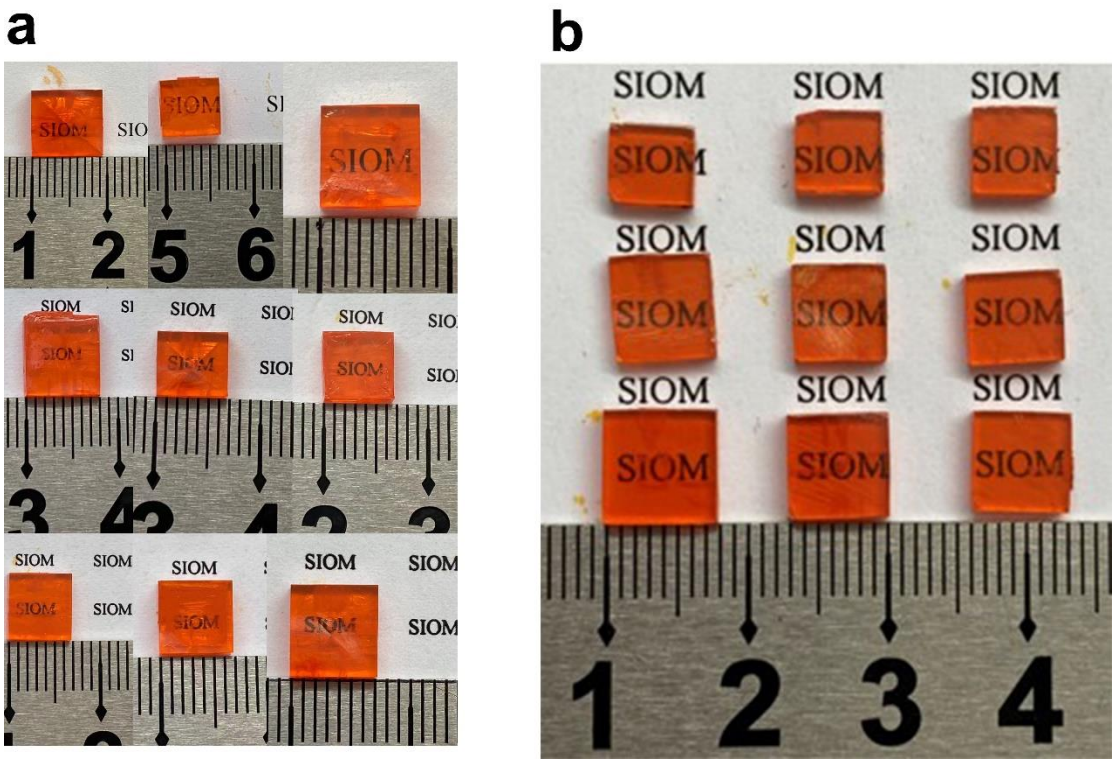

Figure S2. The photographs of (a) as-grown and (b) polished $MAPbBr_3$ crystals.

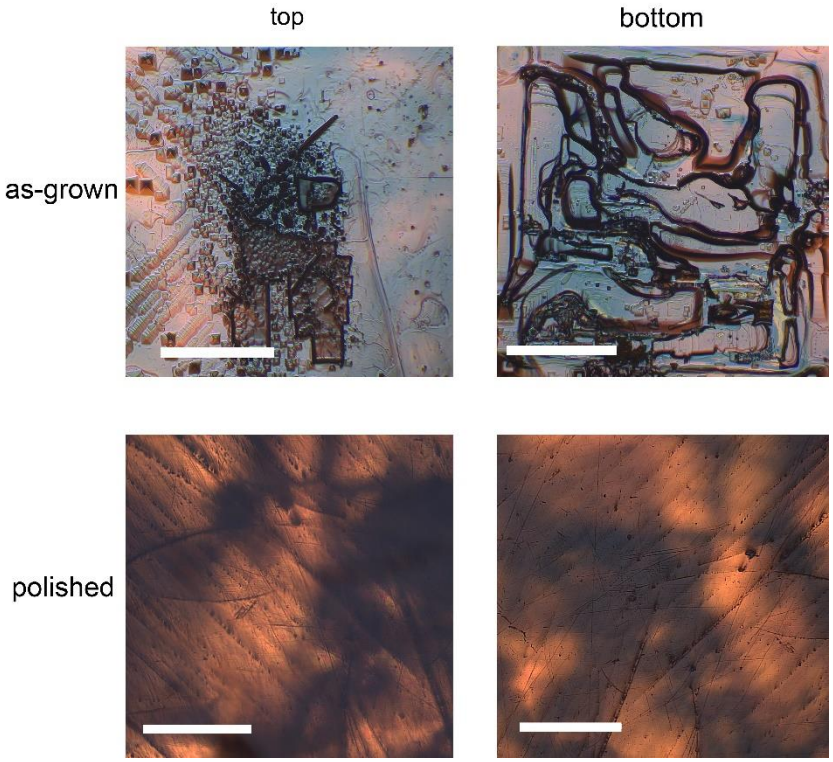

Figure S3. Optical micrographs of top and bottom surface of as-grown and polished $MAPbBr_3$ crystal. The scale bars represent 500 μm.

Figure S4. The photograph of the polished crystal. The edge of the inner seed crystal shows a black outline in the figure.

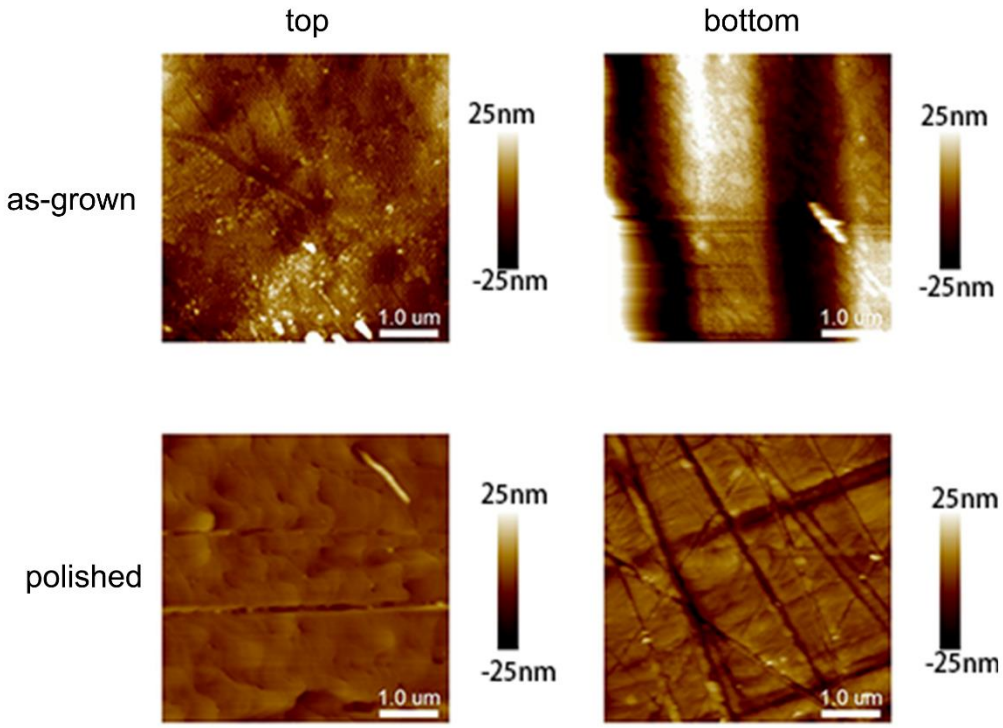

Figure S5. Atomic force microscopy (AFM) images of top and bottom surface of as-grown and polished $MAPbBr_3$ crystal. The scale bars represent and 1 μm.

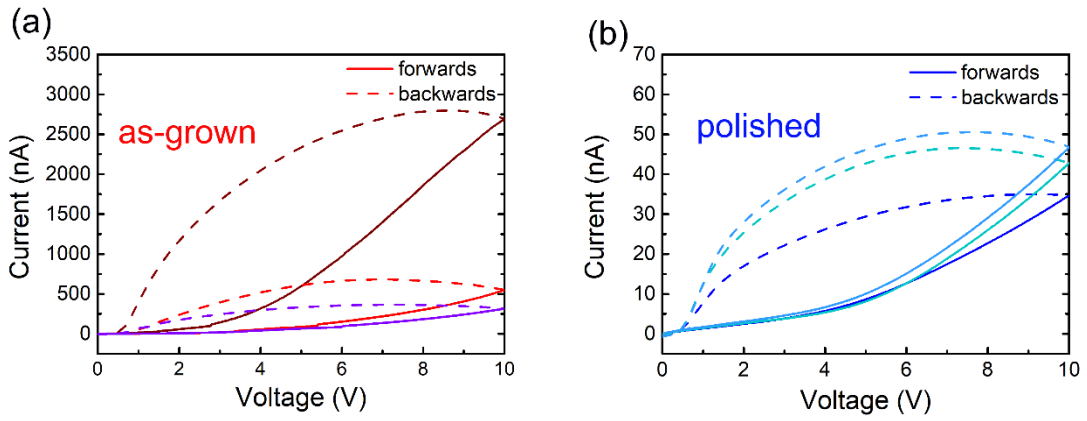

Figure S6. Current - voltage sweep curves of (a) three as-grown and (b) three polished $MAPbBr_3$ crystals.

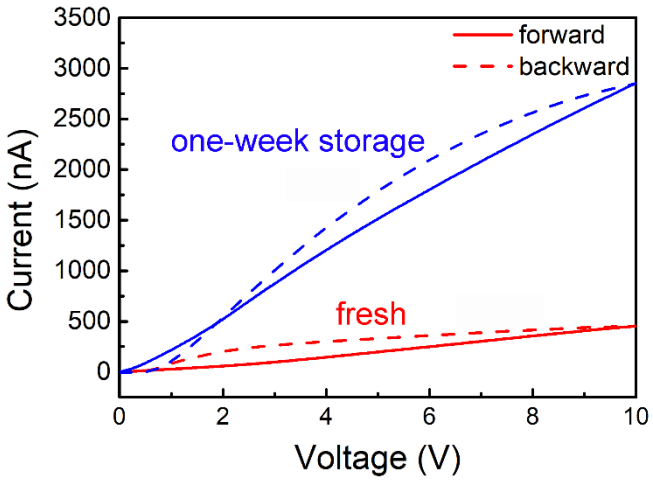

Figure S7. Current - voltage sweep curves of fresh and one-week storage planar device based on as-grown $MAPbBr_3$ crystals.

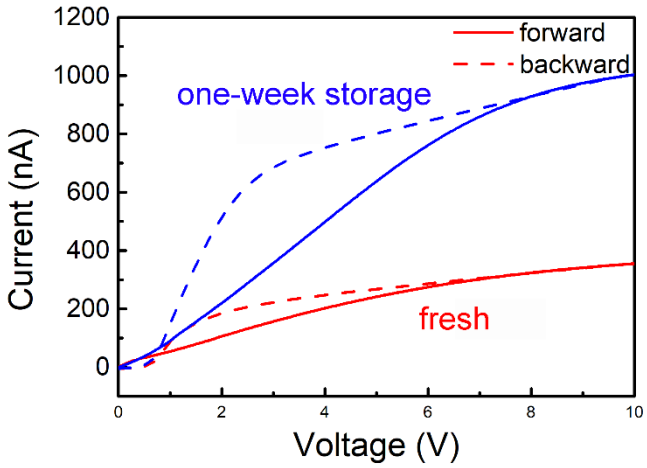

Figure S8. Current - voltage sweep curves of fresh and one-week storage planar device based on $MAPbBr_3$ crystal polished without passivant.

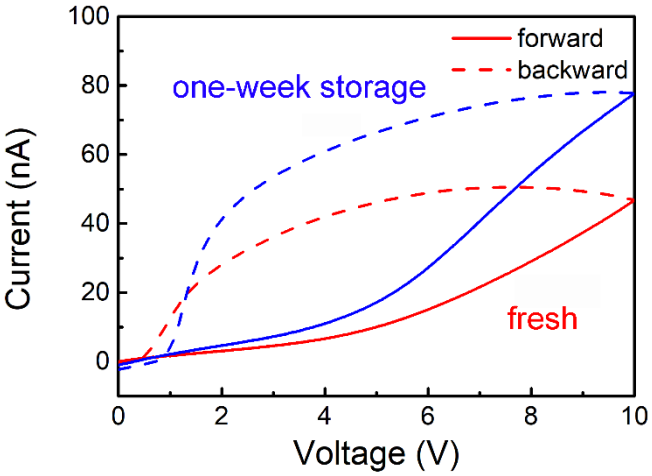

Figure S9. Current - voltage sweep curves of fresh and one-week storage planar device based on $MAPbBr_3$ crystal polished with passivant.

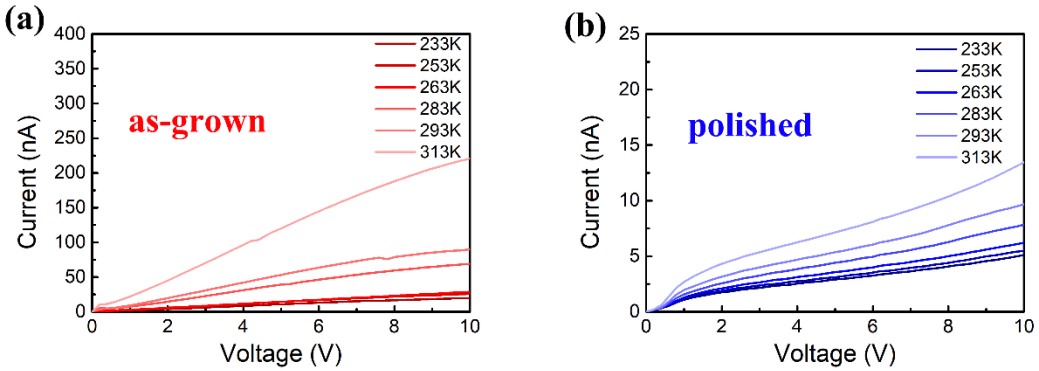

Figure S10. Current - voltage sweep curves of planar device based on (a) as-grown and (b) polished $MAPbBr_3$ crystals at different temperature.

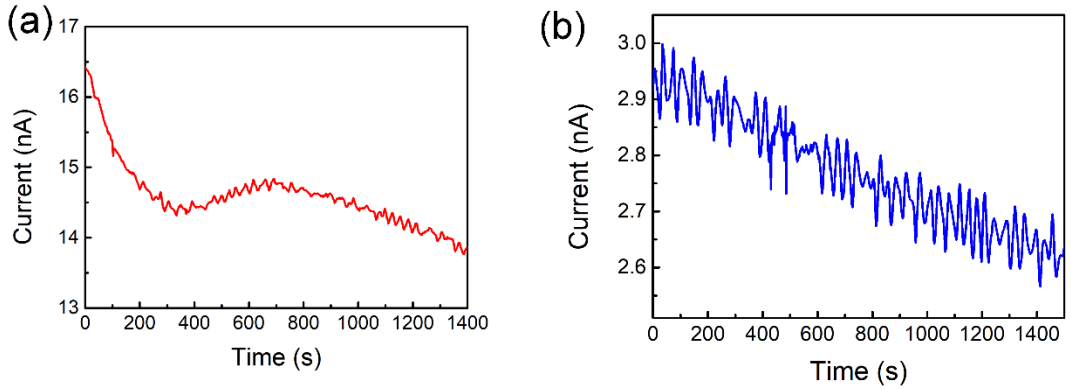

Figure S11. The dark current of the sandwich devices based on the (a) as-grown and (b) polished crystals from 0 to 1400s.

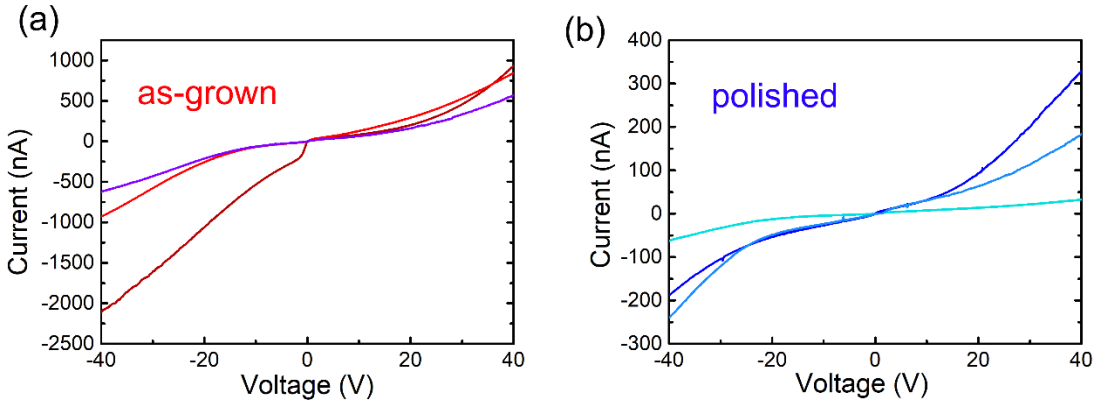

Figure S12. IV sweep curves of three sandwich structure devices based on (a) as-grown $MAPbBr_3$ and (b) $MAPbBr_3$ polished by passivant.

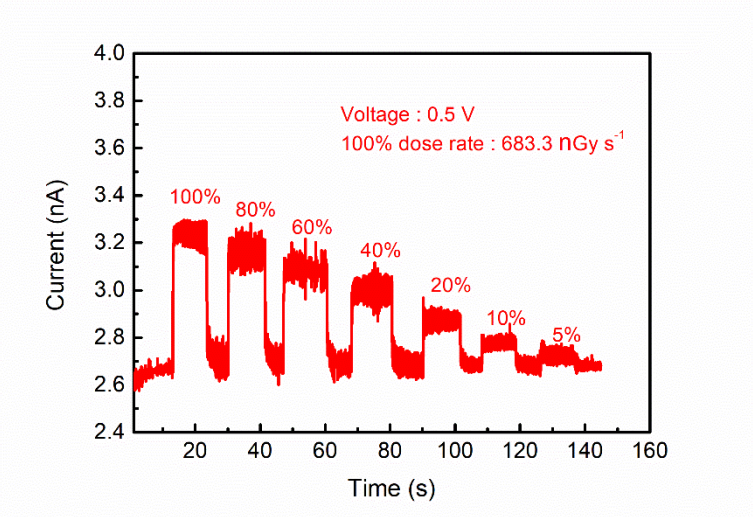

Figure S13. X-ray responses at different dose rates of X-ray detector based on polished $MAPbBr_3$ under 0.5V bias. The maximal dose rate used here is about 683.3 nGy s^{-1}.

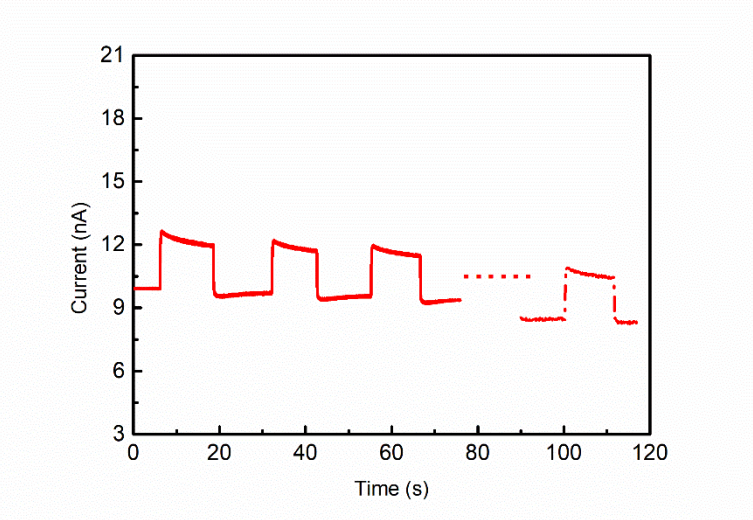

Figure S14. Time dependent response of X-ray detector based on as-grown $MAPbBr_3$ crystal at 0.6833 μGy s^{-1} dose rate under 0.2V. The dashed line pulse occurs after the solid line pulse train. The time corresponding to the dashed pulse in the figure has no practical significance. The figure relates to the figure 5 in the text.

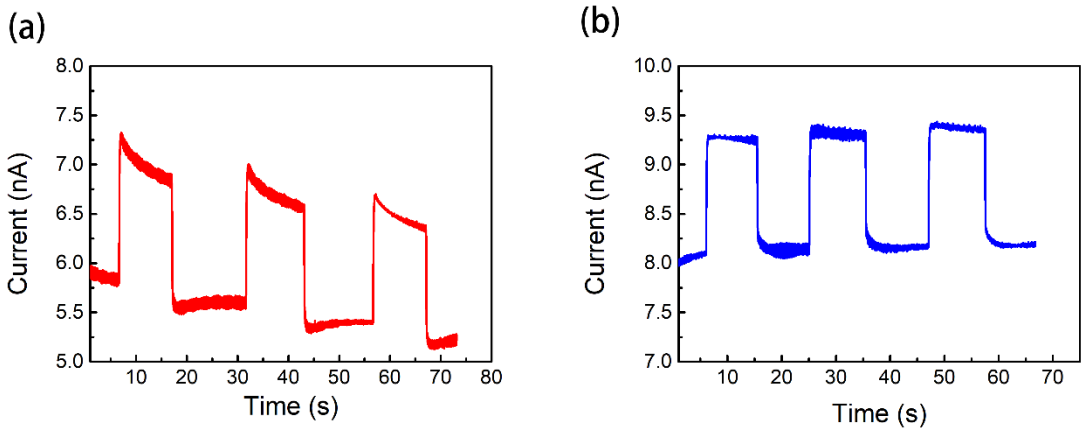

Figure S15. The stability of the devices based on the (a) as-grown and (b) polished crystals under the same radiation response.

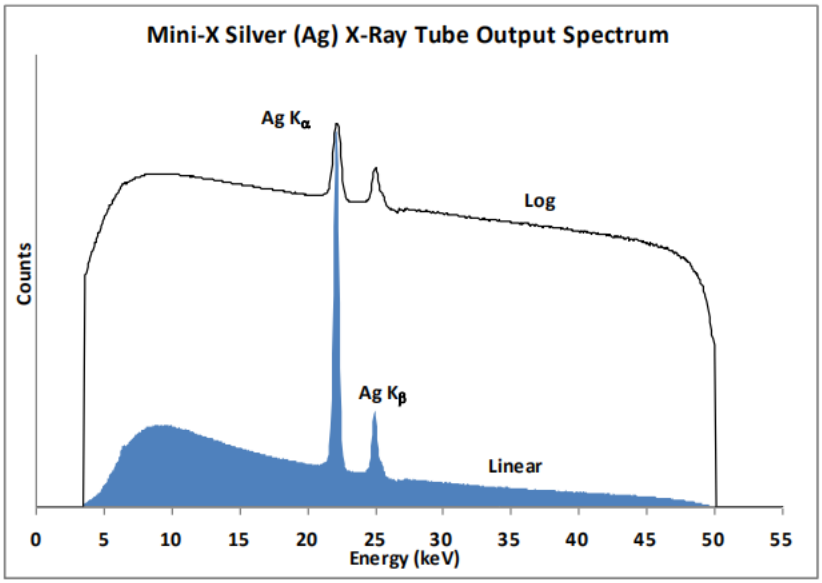

Figure S16. Output Spectrum with silver (Ag) target. This was measured using a 1 mm thick CdTe detector located 1 meter from the Mini-X with a 1 mm pinhole collimator in front of the detector. Reproduced with permission from https://www.amptek.com/products/mini-x2-x-ray-tube. Copyright 2019 AMPTEK, Inc.

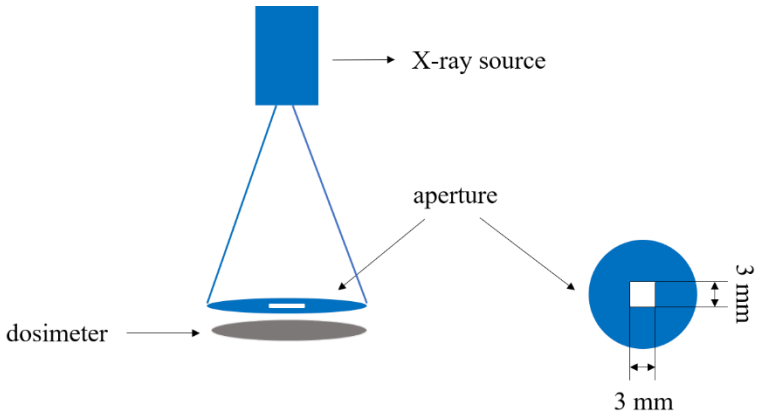

Figure S17. The schematic diagram of the measurement process.

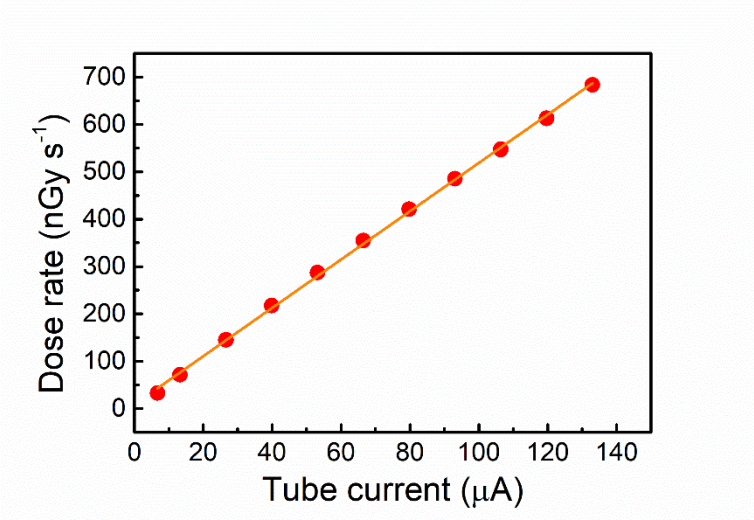

Figure S18. The relationship between dose rate and tube current.

Table 1. Summary of Performance for X-ray Detectors Based on Perovskite.

device structure	sensitivity ($\mu C\ Gy^{-1}\ cm^{-2}$)	detection limit ($nGy\ s^{-1}$)	X-ray (keV)	bias (V/mm)	ref
$Au/MAPbBr_3/C_{60}/BCP/Au$	80	500	50	/	1
$Au/MAPbBr_3/Au$	39.1	/	50	0.5	2
$Al/MAPbBr_3/Au$	359	/	50	14,300	3
$ITO/PEDOT:PSS/MAPbBr_3/C_{60}/BCP/Cu$	632	/	50	~ 5	4
$Au/poly\text{-}TPD/MAPbBr_3/C_{60}/PCBM/Ag$	23,600	/	30	50	5
$Au/BCP/C_{60}/MAPbBr_3/Si$	21,000	36	8	~3.5	6
$Cr/BCP/C_{60}/MAPbBr_{2.94}Cl_{0.06}/Cr$	84,000	7.6	8	60	7
$Au/MAPbBr_{2.5}Cl_{0.5}$ (*p-i-n*)/Au	36,000	16	40	50	8
$FTO/CsPbBr_3/Au$	55,684	215	30	5	9
$Au/Cs_2AgBiBr_6$ /Au	/	59.7	30	2.5	10
$Au/(NH_4)_3Bi_2I_9/Ag$	803	< 55	50	6.5	11
$Cr/PEA_2PbBr_4/Au$	806	42	150	500	12
$Au/MAPbBr_3/Au$	21,897.44	25	30	0.5	this work

References

1. H. Wei, Y. Fang, P. Mulligan, W. Chuirazzi, H.-H. Fang, C. Wang, B. R. Ecker, Y. Gao, M. A. Loi, L. Cao and J. Huang, *Nat. Photonics*, 2016, **10**, 333-339.
2. W. P. Haodi Wu, Nian Liu, Xinyuan Du, Guangda Niu, Jiang Tang, *IEEE Nucl. Sci. Sympos. Medi. Imag. Confer.*, 2019.
3. Q. Xu, W. Shao, Y. Li, X. Zhang, X. Ouyang, J. Liu, B. Liu, Z. Wu, X. Ouyang, X. Tang and W. Jia, *ACS Appl. Mater. Interfaces*, 2019, **11**, 9679-9684.
4. A. Feng, S. Xie, X. Fu, Z. Chen and W. Zhu, *Front. Chem.*, 2021, **9**, 823868.

5. X. Wang, D. Zhao, Y. Qiu, Y. Huang, Y. Wu, G. Li, Q. Huang, Q. Khan, A. Nathan, W. Lei and J. Chen, *Phys. Status Solidi - R.*, 2018, **12**.
6. W. Wei, Y. Zhang, Q. Xu, H. Wei, Y. Fang, Q. Wang, Y. Deng, T. Li, A. Gruverman, L. Cao and J. Huang, *Nat. Photonics*, 2017, **11**, 315-321.
7. H. Wei, D. DeSantis, W. Wei, Y. Deng, D. Guo, T. J. Savenije, L. Cao and J. Huang, *Nat. Mater.*, 2017, **16**, 826-833.
8. X. Wang, Y. Xu, Y. Pan, Y. Li, J. Xu, J. Chen, J. Wu, Q. Li, X. Zhang, Z. Zhao, C. Li, E. E. Elemike, D. C. Onwudiwe, J. Akram and W. Lei, *Nano Energy*, 2021, **89**.
9. W. Pan, B. Yang, G. Niu, K. H. Xue, X. Du, L. Yin, M. Zhang, H. Wu, X. S. Miao and J. Tang, *Adv. Mater.*, 2019, **31**, e1904405.
10. W. Pan, H. Wu, J. Luo, Z. Deng, C. Ge, C. Chen, X. Jiang, W.-J. Yin, G. Niu, L. Zhu, L. Yin, Y. Zhou, Q. Xie, X. Ke, M. Sui and J. Tang, *Nat. Photonics*, 2017, **11**, 726-732.
11. R. Zhuang, X. Wang, W. Ma, Y. Wu, X. Chen, L. Tang, H. Zhu, J. Liu, L. Wu, W. Zhou, X. Liu and Y. Yang, *Nat. Photonics*, 2019, **13**, 602-608.
12. F. Lédée, A. Ciavatti, M. Verdi, L. Basiricò and B. Fraboni, *Adv. Opt. Mater.*, 2021, **10**.